Numerical investigation of strain localization in heterogeneous soft clay under undrained condition

Mona Siahkouhi[1]*, *Franz* Tschuchnigg[2], *Gertraud* Medicus[1], and *Barbara* Schneider-Muntau[1]

[1] Institute of Infrastructure, Computational and Experimental Soil Mechanics, Universität Innsbruck, Austria
[2] Institute of Soil Mechanics, Foundation Engineering and Computational Geotechnics, Graz University of Technology, Austria

1 Introduction

Material inhomogeneity, loading path, and boundary conditions, can be considered as some of the parameters that affect the shear banding process as shown both experimentally and numerically. Siahkouhi et al. [1] studied the impact of inhomogeneity on stress-strain behaviour of simulated drained biaxial tests with spatially varying soil parameters and showed that higher level of inhomogeneity led to more obvious shear strength reduction. Biaxial and triaxial tests on fine grain soil, often run under both drained and undrained conditions, reveal that plane strain specimens exhibit one or more steeply inclined shear bands (usually at 50–60° to the horizontal), with measured band thicknesses of about 6–10 mm using digital image correlation [2]. In contrast, triaxial compression tests (axisymmetric loading, generally with rubber membrane confinement and lubricated or fixed platens) more often display diffuse deformation, with bulging and sometimes multiple, less-defined shear zones. Shear bands in triaxial tests tend to form later (often after peak stress) and may be less steep, depending on end friction and sample geometry [3]. Drainage conditions further modulate localization. In drained plane strain tests, overconsolidated clays consistently show a sharp peak in the stress–strain curve, followed by post-peak softening and clear shear band formation [2]. In undrained tests, normally consolidated clays tend to form wider shear zones, with positive excess pore pressure, whereas overconsolidated or structured clays, which may generate negative pore pressures (where negative excess pore pressure denotes a reduction in pore water pressure) upon dilation like behaviour may show a brittle failure by narrow, well-developed shear bands [3-5]. Studies also show that higher confining pressures and faster strain rates in plane strain tests can modestly increase shear band thickness and steepen the inclination due to enhanced pore pressure effects [3]. As a conclusion it can be noted that, the presence of material inhomogeneity, boundary conditions, loading rate and many other parameters affect the strain localization and shear banding process.

In continuation of the previous studies, the present study numerically investigates the influence of material inhomogeneity and boundary condition on strain localization in consolidated undrained soft clay using coupled hydro-mechanical finite-element simulations. The results show that inhomogeneity reduces peak shear strength and enhances pore-pressure buildup and post-peak softening, while biaxial and triaxial test's simulations lead to distinct localization patterns.

2 Numerical modelling

In the current study the FE software ABAQUS 2019 was utilized for numerical modelling. In order to capture the undrained behaviour of the clayey material porous elastic-clay plasticity model was assigned which is an extension of the cam clay model developed by Roscoe et al. [6]. The clay plasticity model describes the inelastic behaviour of the material by a yield function depending on the three stress invariants, an associated flow assumption to define the plastic strain increment, and strain hardening behaviour. The elastic part of the deformation is defined by the porous elastic material model which is a non-linear, isotropic elasticity model and is well suited for small elastic strains. The undrained behaviour in the multi-element models was simulated by utilizing a hydro-mechanical coupling approach and impermeable outer boundaries of the sample.

The considered material (Weald clay), is a sedimentary formation from the Early Cretaceous period, predominantly found in Southeast England. The clay exhibits high plasticity and the permeability is often measured in the range of 10^{-6} to 10^{-9} m/s [7]. These properties make it a critical material in geotechnical engineering. The input parameters for the porous elastic-clay plasticity constitutive model of this material are presented in Table 1 [8].

Table 1. Material parameters [8].

Parameter	Symbol	Value
Intersection of NCL with p' = 1 kPa in e - lnp' space	e_0	1.1
Slope of the critical state line in e - lnp' space	λ	0.093
Slope of the unloading, line in e - lnp' space	κ	0.035
Slope of critical state line in p' - q space	M	0.95
Poisson's ratio	ν	0.28

* Corresponding author: mona.siahkouhi@uibk.ac.at

Biaxial 2D tests were simulated as multi-element test with 5000 CPE8P elements, biaxial and triaxial 3D tests were simulated with 250000 C3D20P elements. Void ratios = 0.6, representing OCR = 3.45 respectively, were assigned for the homogeneous model (HM) and mean void ratios e_{mean} = 0.6 ($\mathrm{OCR}_{\mathrm{mean}}$ = 3.45) with a standard deviation in void ratio of 0.005 were used for the inhomogeneous model (IM) simulations. In order to apply the inhomogeneity, a random normal distribution of void ratio across the elements of the 2D and 3D models was considered that represents the variation in soil's density. Based on the assigned value of initial void ratio e_{ini} for each element, the equivalent preconsolidation pressure $p'_{\mathrm{c,ini}}$ (maximum mean effective stress in loading history of soil) as illustrated in Figure 1, with the confining pressure p'_{ini} = 100 kPa can be defined as:

$$p_{\mathrm{c,ini}} = \exp\left(\frac{e_0 - e_{\mathrm{ini}} - \kappa \ln p_{\mathrm{ini}}}{\lambda - \kappa}\right) \tag{1}$$

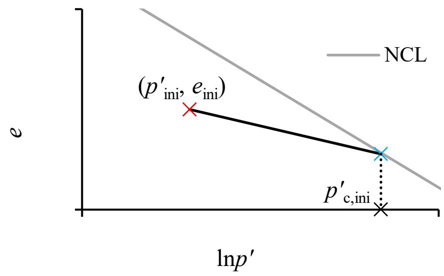

Figure 1. Schematic sketch of preconsolidation pressure in e-lnp' space.

Inhomogeneities in initial void ratio affect not only the initially size of the implemented yield surface but also the soil's permeability k_{ini}. Since the permeability of the soil is void ratio-dependent, this parameter is also determined for the assigned void ratios by using the following equation suggested by Tavenas et al. [9], where C_k is the permeability index that describes how sensitive a soil's permeability k_{ini} is to changes in void ratio e_{ini} and k_0 and e_0 are known permeability and void ratio values.

$$k_{\mathrm{ini}} = k_0 10^{-\frac{e_{\mathrm{ini}} - e_0}{C_k}} \tag{2}$$

With k_0= $1.01 \cdot 10^{-7}$ m/s based on the ranges given by Clark [7] and $C_k = 0.5 e_0$ according to Achari & Joshi [10].

In the 3D triaxial simulations, the lateral boundaries are free to move, while in the 2D and 3D biaxial simulations the front and back boundaries are fixed in one horizontal direction and the left and right boundaries remain free horizontally. The bottom boundary is fixed in all directions. The specimens' dimensions are assumed to be 0.05 and 0.1 m in horizontal (x and z) and vertical (y) directions, respectively. Displacement-controlled shearing is applied by prescribing a vertical displacement at the top boundary. Considering the fact that localization simulations are mesh-dependent [11, 12], in this study a consistent framework, utilizing regular mesh with the same mesh size and number of elements for HM and IM simulations is used to allow for a direct comparison of localization patterns.

All the analyses were performed as undrained, coupled simulations consisting of a consolidation phase and a shearing step with the total displacement of the top of 0.02 m and at a rate of 0.02 mm/s. During the consolidation phase, the top boundary was defined as a drained boundary by prescribing zero pore pressure. The step duration was chosen sufficiently long for excess pore pressures to dissipate to approximately zero. During the shearing step, all external boundaries were defined as impermeable, so that no drainage could occur across the specimen boundaries and the response remained globally undrained. At the same time, spatial redistribution of pore pressure within the domain through continuity of the interpolated pore-pressure field is allowed.

3 Results

This section provides an evaluation of the simulations of inhomogeneous and homogeneous undrained models under biaxial and triaxial conditions. The discussion is structured to address the impact of inhomogeneity and boundary condition on the soil response, localization patterns and formation of shear bands.

Experimental and numerical studies have reported spatial heterogeneity in soil specimens, reflected by local variations in material properties [2, 4]. All the stresses, strain, excess pore pressure and void ratio values are presented as specimen-averaged quantities, obtained by averaging over all integration points. We refer to these values as the global values and present them throughout the global responses e.g. stress paths and stress-strain curves.

Figure 2 compares the global response of the HM and IM simulations for an initial OCR and $\mathrm{OCR}_{\mathrm{mean}}$ of 3.45. In Figure 2a the global stress-strain behavior of the HM and IM is illustrated in terms of deviatoric stress q and the invariant strain measure ε_{q} (deviatoric strain). It can be seen that the IM mobilizes about 10% lower peak strength compared to the HM. In the post peak state, the HM shows only limited softening and then a nearly constant residual level, whereas the IM displays a clear continued decrease in q with increasing ε_{q} that can be potentially attributed to the shear band formation.

The global excess pore pressure u response in Figure 2b demonstrates that both IM and HM generate positive u rapidly up to the peak, but the HM shows a pronounced reduction of u immediately after the peak, reaching a constant level. However, IM shows higher u at the peak and during the post-peak state and reduces more gradually. Figure 2c indicates that HM not only attains higher deviatoric stress q but also reaches higher mean effective stress p' compared to IM as the shearing occurs. This behavior can be attributed to pore pressure increment due to strain localization and shear band development. In the e–p' plane (Figure 2d), both simulations evolve toward the critical state line (CSL). The HM reaches the critical void ratio and the CSL, whereas IM does not reach the CSL indicating that in an inhomogeneous FEA after the shearing not all the elements reach their critical state.

Figure 3 shows the deviatoric strain distribution pattern at 60 %, 100 %, and 200 % of the peak deviatoric strain ($\varepsilon_{q,p}$) for IM, that are shown with red X-marks in Figure 2. At 60% of $\varepsilon_{q,p}$, the strain distribution is almost homogeneous within the soil, while the top and bottom boundaries are slightly affected and show an inhomogeneous distribution. However, no clear shear band is observed. At the peak level, the IM exhibits pronounced strain localization, with multiple localized bands and the impact of boundaries are diminished (smaller localization zone) in comparison to the previous stage. At 200 % of $\varepsilon_{q,p}$, two clear shear bands become dominant and the IM develops an X-shaped shear band pattern.

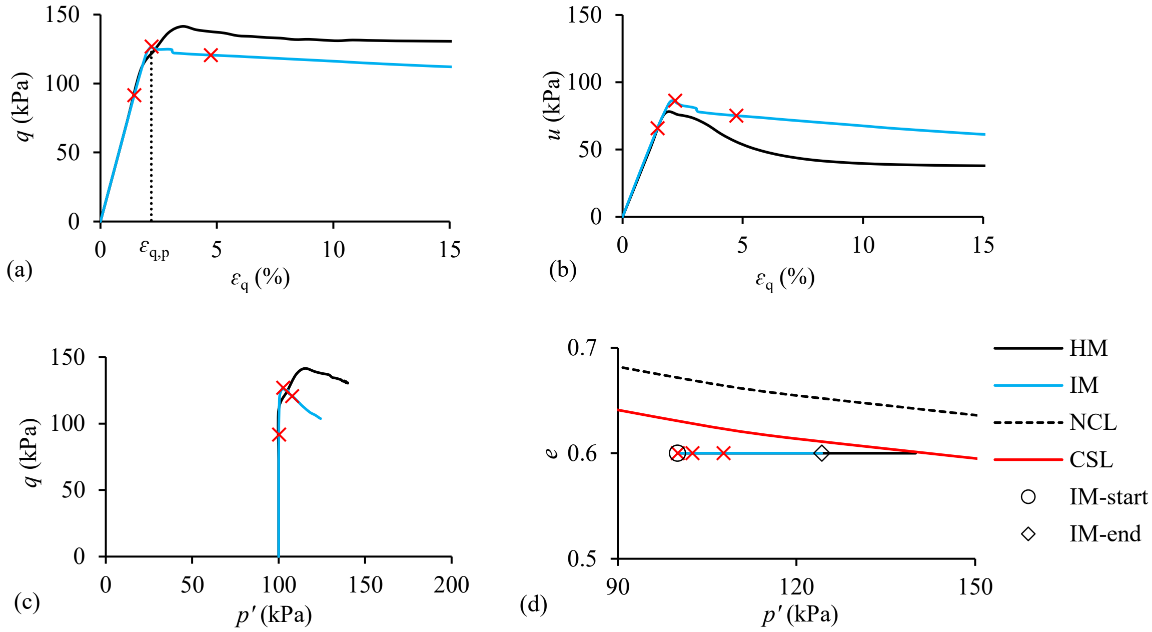

Figure 2. Evolution of the (a) deviatoric stress q (b) excess pore pressure u with respect to the deviatoric strain ε_q (c) q with respect to mean effective stress p' and (d) evolution of the void ratio with respect to p' for IM and HM simulations of plane-strain biaxial tests with initial OCR and OCR_{mean} of 3.45.

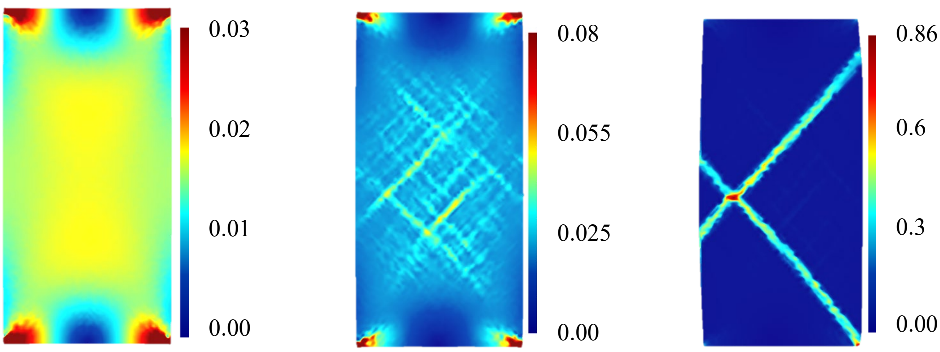

Figure 3. Distribution of deviatoric strain ε_q inside the soil in biaxial test of IM simulations with initial OCR_{mean} of 3.45, at 60, 100 and 200 % of $\varepsilon_{q,p}$.

Figure 4 shows the deviatoric strain localization pattern in homogeneous and inhomogeneous 3D simulations of biaxial and triaxial tests for OCR and OCR_{mean} = 3.45 at 5 % of global axial deformation. As it is shown in Figure 4a and 4c, the localization pattern in triaxial and biaxial HMs is symmetric, whereas in both IMs (Figure 4b and 4d) it is unsymmetric due to inhomogeneity presence. Under plane strain condition in biaxial tests, HM exhibits an X-shaped pattern, consisting of two narrow shear bands, typical for plane-strain condition [11], while IM illustrates an asymmetric single inclined shear band with a thinner localized zone. In triaxial test simulations, HM exhibits a more diffused localization pattern in a wider area. In contrast, IM forms an irregular, inclined localization zone.

It can be noted that 3D triaxial models show a bulging (HM, Figure 4c) and buckling (IM, Figure 4d) failure modes, are characterized by diffuse and globally distributed deformation, where strain spreads over a relatively broad zone without forming a distinct, narrow localization plane. However, the biaxial simulations tend to form clear shear bands, where deformation localizes abruptly into one or a few well-defined, inclined zones which is typical for plane-strain condition [3, 11] and inhomogeneity leads to asymmetric shear banding patterns.

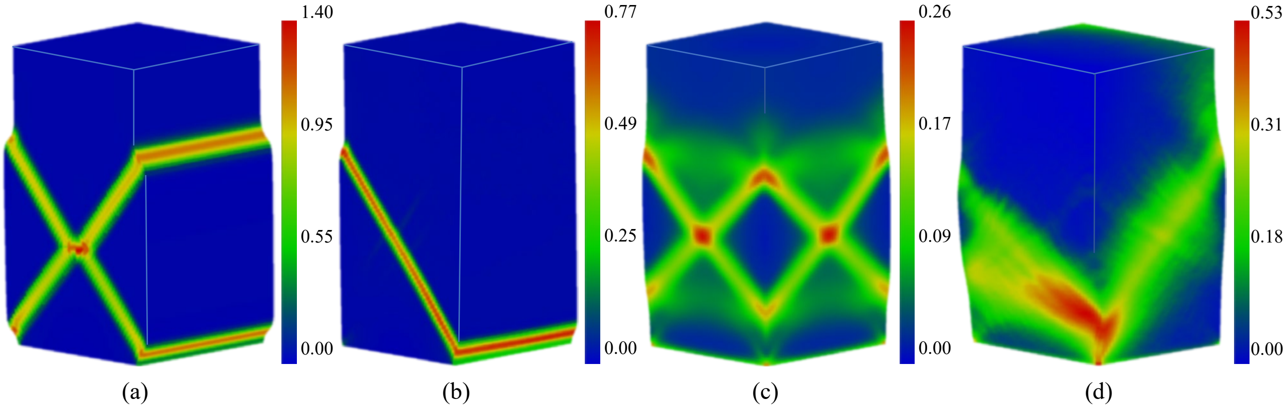

Figure 4. Distribution of deviatoric strain ε_q inside the soil for (a) HM and (b) IM biaxial, (c) HM and (d) IM triaxial simulations with initial OCR and OCR_{mean} of 3.45 at 5 % global axial deformation, respectively.

4 Conclusion

This study aimed to investigate the effects of inhomogeneity and boundary condition on strain localization and shear band formation of undrained 2D and 3D biaxial and 3D triaxial tests. The undrained behaviour has been modelled by fully coupled calculations utilising clayey material with the modified Cam clay model. The key findings can be summarized as follows:

- Considering the inhomogeneity in FEA simulations leads to a reduction of peak shear strength, gaining higher excess pore pressure and more pronounced post-peak softening caused by the formation of localized zones.
- Localization patterns of 3D homogeneous model and inhomogeneous model simulations reflect the significant effect of inhomogeneity on soil deformation.

In conclusion, the results show that strain localization in undrained soft clays is strongly controlled by soil inhomogeneity and boundary conditions. The imposed stress condition strongly influences strain localization: plane-strain (biaxial) loading and triaxial loading produce different modes of shear-band formation, including differences in the onset, orientation, and subsequent development of the bands.

References

1. M. Siahkouhi, G. Medicus, F. Tschuchnigg, B. Schneider-Muntau, Investigating the impact of inhomogeneous soil parameters on shear strength in biaxial tests, in Proceedings of the 28th European Young Geotechnical Engineers Conference (2024), pp. 1–9.
2. T.Y. Kwak, K.H. Park, J. Kim, C.K. Chung, S.H. Baek, Shear band characterization of clayey soils with particle image velocimetry. Appl. Sci. **10**, 1139 (2020). https://doi.org/10.3390/app10031139
3. B. Liu, L. Kong, C. Li, J. Wang, Evolution of shear band in plane strain compression of naturally structured clay with a high sensitivity. Appl. Sci. **12**, 1180 (2022). https://doi.org/10.3390/app12031180
4. K.A. Alshibli, I.S. Akbas, Strain localization in clay: Plane strain versus triaxial loading conditions. Geotech. Geol. Eng. **25**, 45–55 (2007). https://doi.org/10.1007/s10706-006-0005-4
5. Dueck, L. Börgesson, L.E. Johannesson, Stress-strain relation of bentonite at undrained shear. Laboratory tests to investigate the influence of material composition and test technique, SKB Report SKB-TR-10-32, Swedish Nuclear Fuel and Waste Management Co., Stockholm (2010).
6. K.H. Roscoe, A. Schofield, A. Thurairajah, Yielding of clays in states wetter than critical. Géotechnique **13**, 211–240 (1963). https://doi.org/10.1680/geot.1963.13.3.211
7. J. Clark, Performance of a propped retaining wall at the Channel Tunnel Rail Link, Ashford, Ph.D. thesis, University of Southampton (2006).
8. V. Navarro, M. Candel, A. Barenca, A. Yustres, B. Garcia, Optimisation procedure for choosing cam clay parameters. Comput. Geotech. **34**, 524–531 (2007). https://doi.org/10.1016/j.compgeo.2007.01.007
9. F. Tavenas, P. Jean, P. LeBlond, S. Leroueil, The permeability of natural soft clays. Part II: Permeability characteristics. Can. Geotech. J. **20**, 645–660 (1983). https://doi.org/10.1139/t83-073
10. G. Achari, R.C. Joshi, A reexamination of the permeability index of clays: discussion. Can. Geotech. J. **31**, 140–141 (1994).
11. Y. Li, S. Anyuan, F. Zhu, A review of theoretical, experimental and numerical advances on strain localization in geotechnical materials. Appl. Sci. **15**, 12154 (2025). https://doi.org/10.3390/app152212154
12. H. Tang, Y. Li, Z. Hu, X. Song, Numerical simulation of strain localization through an integrated Cosserat continuum theory and strong discontinuity approach. Comput. Geotech. **151**, 104951 (2022). https://doi.org/10.1016/j.compgeo.2022.104951